DOI: 10.65731/ama/2026-0063 *acta mechanica et automatica, vol. 20 no.3 (2026)*

HIGH-SPEED MACHINING OF NICKEL-BASED ALLOY INVAR 36: OPTIMIZATION OF MACHINING VIBRATION, TOOL, AND ALLOY SURFACE CHARACTERISTICS

Sushmith Shetty M*, Vikas MARAKINI, Grynal D'MELLO*, Gururaj BOLAR*****

*Nitte (Deemed to be University), NMAM Institute of Technology (NMAMIT), Nitte,
Department of Mechanical Engineering, Mangalore, India, 575018
**College of Science and Engineering, Ritsumeikan University, 1-1-1 Nojihigashi, Kusatsu-shi, Shiga, Japan, 525-8577
***Manipal Institute of Technology, Manipal Academy of Higher Education, Manipal, India, 576104

sushmith.shettym@gmail.com, vikasbhat02@gmail.com, grynal@nitte.edu.in, Gururaj.bolar@manipal.edu

received 28 April 2026, revised 22 July 2026, accepted 27 July 2026

Abstract: INVAR 36 is considered a difficult to machine alloy because of its physical properties, but it has a low coefficient of thermal expansion and good dimensional stability that makes it suitable for aerospace, precision engineering, and tooling applications. Dry turning experiments have been done on INVAR 36 based on different cutting speeds (v_c), feed rates (v_f), and depth of cuts (a_p) with respect to their influences on surface roughness (R_a), maximum flank wear (VB_{max}), and machining vibrations, Root Mean Square. Through Response Table Analysis, feed rate was found to be the highest influencing parameter for surface roughness, while cutting speed was the highest influencing parameter for tool wear and vibrations. Further, the vibration data have been studied through Fast Fourier Transform in frequency, domain with the dominant frequency being 105.6 Hz at optimal machining conditions. The optimization was carried out through multi-criteria decision-making by employing Grey Relational Analysis, Evaluation based on Distance from Average Solution, and Additive Ratio Assessment. It is seen that all three approaches gave the same optimum machining parameters, and hence the validity of the optimum machining parameters can be said to be reliable. The optimum combination of the parameters was found to be v_c = 150 m/min, v_f = 0.18 mm/rev, and a_p = 1.2 mm, giving the minimum RMS vibration value of 14.246 g and flank wear of 0.110 mm.

Keywords: Invar 36, dry turning, machining vibration, root mean square (RMS); tool wear; fast Fourier transform (FFT), multi-criteria decision-making (MCDM), process optimization

1. INTRODUCTION

Nickel-based alloys (often called Ni-based superalloys) are trending in both research and industry because they perform exceptionally well in extreme environments. Nickel-based alloys are high-performance materials designed for extreme environments, offering superior protection against corrosion, oxidation, and, often, high-temperature creep [1]. These properties make them essential for several rapidly growing technologies. Primarily alloyed with elements like chromium, molybdenum, and iron, they are critical in industries such as aerospace (jet engines, rocket engines, and exhaust systems), power generation (gas turbines, nuclear reactors, and heat exchangers), and processing (Chemical processing, oil and gas extraction, and pollution control equipment) [1,2]. Fe-Ni alloys like Invar 36 as well as nickel-based superalloys are considered to be hard-to-cut materials due to their high hardness, work-hardening nature, adhesiveness, and comparatively lower thermal conductivity that contribute to heat accumulation in the machining region [3]. The consequence of the mentioned properties is an increase in cutting temperature, cutting forces, tool wear rate, and deterioration of machining process performance [4]. It was found that adhesion, abrasion, diffusion, and coating degradation were the main wear modes occurring during machining, whereas the effect of cutting speed and feed rate on tool wear rate and surface quality was considerable [5]. Besides, the thermal and mechanical loads developed during machining process cause the increase in force fluctuations and dynamic instability leading to vibration intensification and faster tool wear [6]. Invar, also known as Invar 36 or FeNi36 (roughly 64% iron, 36% nickel), is recognised for its uniquely low thermal expansion. This makes it an attractive option for manufacturers in applications where the temperature variations are extreme [7-10]. Invar 36, although very effective and widely in demand, presents difficulties during machining. Invar 36 is considered difficult to machine because it is ductile and has low thermal conductivity, leading to rapid tool wear, stringy chips, and high heat buildup [11].

Process variables such as speed, feed, and cutting depth are crucial and significantly influence material removal rate and surface finish in machining operations [12]. Conventional machining is an important operation where machining takes place at room temperature without the use of any coolant or cutting fluids. It has many economic and environmental advantages as it helps in reducing machining costs and hence the environmental effects related to the disposal of cutting fluids [13]. In machining operations, the roughness attained on the surfaces has significant effects on the efficiency of the machined components and the quality of the product. Machining parameters, along with tool-related parameters comprising tool wear and tool geometry, have major effects on the obtained surface roughness [14]. Surface roughness may also be significantly impacted by characteristics of the work material, such as hardness and grain size [15]. Some research has indicated that decreased roughness also enhances the corrosion resistance, thus requiring a finer surface to maximise the protective effect against the corrosion [16].

In machining operations, the wear mechanism is an important factor since it directly affects tool life, efficiency of machining, and the obtained surface quality of the component. Tool wear may occur by different mechanisms such as abrasion, adhesion, chemical, thermal, or mechanical phenomena [17]. Also, the relationship assessment between tool behaviour and the vibration during machining operation is a critical area of research. Vibration of higher magnitude may lead to a reduction in machined performance, increased tool wear, and poorer surface quality of the component. In this regard, tool wear has often been assessed through statistical measures in terms of Root Mean Square (RMS) values of the vibration signals [18]. Experimental studies have indeed validated the vibration signal as a method of monitoring tool wear, showing a good relationship between the development of tool wear and the characteristics of vibration [19,20].

A full factorial design is an extensive experimental procedure for studying the effects brought about by multiple factors on machining performance. It involves conducting experiments for all possible combinations of factor levels. It provides the possibility of a thorough study of the interactions between machining factors [21]. The multi-criteria decision-making techniques, also known as Multi-criteria decision-making (MCDM) techniques, are highly effective in solving complex optimization problems in machining because of their capability to accommodate different inconsistent criteria. This attribute is extremely useful in machining studies, where the optimization of process variables is a must in order to attain the required results, including reduced surface roughness, minimum tool wear, and machining vibration, etc. [22]. The complexity in relationships among the variables can be solved through MCDM techniques such as Grey Relational Analysis (GRA), Distance from Average Solution (EDAS), and Additive Ratio Assessment (ARAS) [23].

Current studies on machining Invar 36 are very limited. Zang et al. [24] investigated the chip formation and chip-flow behavior during the machining of Invar36. Orthogonal cutting experiments were performed, mechanical properties and deformation behavior were measured, and the chip morphology and microstructure were analyzed. A flow stress constitutive model was developed based on material tests, a polycrystalline finite element modelling was used to simulate chip formation, and the stress distribution and deformation patterns were analyzed during cutting. It was noted that, increasing cutting speed leads to higher plastic deformation rates, increased shear localization, and more frequent and pronounced serrated chips. Khanna et al. [25] employed Taguchi's methodology to machine INVAR 36 alloy using the end milling process. Optimizing the process variables to achieve minimum roughness was the objective of the study. They found the cutting depth as the major influencing factor affecting the roughness of the alloy, followed by speed and feed, respectively. Based on the identification of specific optimal parameters, they were able to achieve an optimal quality surface with a low surface roughness value of 0.1835 µm. Mahir et al. [26] investigated the machinability of Invar36 during turning using three types of carbide cutting inserts, namely Uncoated carbide inserts, AlTiN coated carbide insert (single-layer coating), TiCN–Al_2O_3 coated carbide insert (multi-layer coating). Machining was conducted to evaluate tool performance based on four main responses, such as cutting force, surface roughness, tool flank wear, and power consumption. The multilayer coated insert performed the best among the three tools. Tool wear reduced by up to 30% compared with single-layer coated insert, up to 60% compared with uncoated insert. The multilayer coated insert also produced the lowest surface roughness. Uncoated inserts showed higher roughness due to rapid tool wear and adhesion effects.

Jovicic et al. [27] investigated dry turning of Inconel 601, which is known for poor machinability. The objective of the study was to model the machining process, optimize machining parameters, and achieve a balance between roughness, flank wear, MRR using optimization approach. It was observed that increasing the feed and speed increased the value of MRR, but increasing the feed adversely affected roughness and flank wear. Feed had one of the strongest influences on all three outputs of the study. Overall, they proposed a hybrid ANN–GA optimization framework, showing that proper control of feed, speed, and tool geometry can simultaneously improve surface finish, tool life, and productivity with prediction errors below 2%. D'Mello et al. [28] performed an experimental work to analyze the effect of cutting vibrations on roughness in high-speed turning of Ti-6Al-4V. Remarkably, they observed that with increased tool wear, the surface quality improved. Feed had a significant effect on roughness responses R_a and R_t, explaining more than 70% variation in results. Rao et al. [29] aimed to optimize turning parameters during machining of Inconel 718. They tried to simultaneously improve multiple responses such as roughness, tool wear, MRR using two MCDM techniques namely, GRA and Technique for Order of Preference by Similarity to Ideal Solution (TOPSIS). Both GRA and TOPSIS successfully optimized turning parameters. The two methods produced different optimal parameter combinations. GRA provided an optimal condition for better improvement in surface roughness and tool wear. Whereas the TOPSIS provided a condition that resulted in a higher material removal rate.

Eskandari et al. [30] conducted a study to optimise machining parameters during the turning of N-155 alloy. The main goal was to simultaneously optimise multiple machining responses using GRA combined with the Taguchi method. The optimal parameter combination identified using GRA provided good results. Abbed et al. [31] conducted a study to investigate the effect of tool materials and process variables on the turning performance of titanium alloy. The goal of the study was to model and optimize machining conditions using statistical analysis and several MCDM methods such as CoCoSo, MABAC, ARAS, and CODAS. Feed rate strongly affected surface roughness. Speed and cutting depth significantly influenced cutting forces. Tool material also had a noticeable effect on machining performance. The ranking results from CoCoSo, MABAC, ARAS, and CODAS were largely consistent, which confirmed the reliability of MCDM approaches for machining optimization. Sivalingam et al. [32] investigated the machining of Inconel 718 during the turning process. The main goals of the study were to improve surface quality, increase tool life, and identify optimal machining parameters. To achieve this, they applied MCDM techniques such as ARAS and CODAS. Both MCDM methods produced similar optimal solutions, validating the reliability of the optimization approach.

Although there are few relevant studies available in the current scenario related to Invar 36, there is a substantial research gap in the current literature with respect to a complete comparative study of surface roughness, tool wear, and machining vibration, and MCDM approaches, particularly in the context of turning operations with Invar 36. This work addresses the gap in the literature by providing an in-depth quantitative analysis for the dry turning of alloy Invar 36. The research adopts a full factorial experiment design with three levels, which combines the values of R_a and VB_{max} measured after every pass with the measured vibrational signals. The application of GRA, EDAS, and ARAS offers an overall optimization strategy that can be applied for evaluating the impact of multiple machining responses during the dry turning of Invar 36. Therefore, the objective of this research is to conduct experiments on the influence of cutting speed (v_c), feed rate (v_f), and depth of cut (a_p) on surface roughness (R_a), VB_{max} (maximum flank wear) and machining vibration (RMS) when dry turning of Invar 36 in the case of high-speed machining process. Furthermore, FFT-based frequency domain analysis is used for exploring the dynamics of the machining process and giving mechanistic interpretation of the relationship between tool wear, vibration, and surface roughness.

2. METHODOLOGY

The methodology of the study has been depicted in Fig. 1.

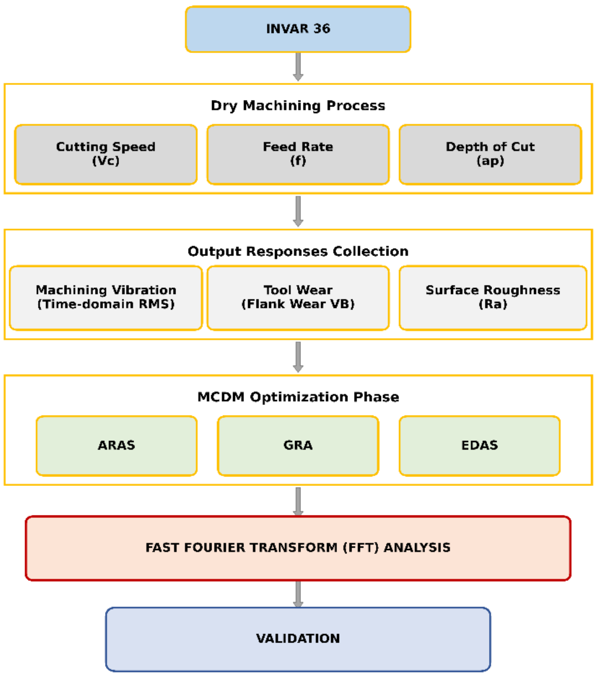

Fig. 1. Methodological framework of the study

2.1. Experiments

The alloy was received as a cylindrical rod measuring 220 mmx50 mm. The specifics of the alloy Invar 36 are displayed in Tab. 1. Fig. 2. (a) presents the XRD pattern of the alloy, where the hkl indices are recognized as 111, 200, 220, 311, and 222, which are from the Austenitic FCC phase of the composition, identified at 52°, 60°, 89°, 111°, and 119°, respectively [33]. The microstructure of the alloy surface taken from a Scanning Electron Microscope (FESEM) (GEMINI300) is presented in Fig. 2 (b). The microhardness of the raw material (as-received) is found to be 220 HV.

The engine lathe used for this process has a maximum speed of 1,800 RPM and a 10 HP motor. The spindle speed can be accurately controlled by a 3.7 kW (5 HP) AC inverter drive equipped with a motor-operated potentiometer (MOP). Since the engine lathe allows the spindle speed to be varied in a limited number of preset values, the inverter AC drive is necessary to dynamically vary the spindle speed in RPM to the dynamically decreasing diameter of the workpiece during the machining operation. The AC inverter motor allows the dynamic variation of the cutting speed to be translated to a dynamic variation of the feed rate. This is necessary to ensure that the spindle speed is varied accurately, thus maintaining a constant MRR. The implementation of the AC inverter motor is necessary to ensure that the results of experiments are accurate and precise.

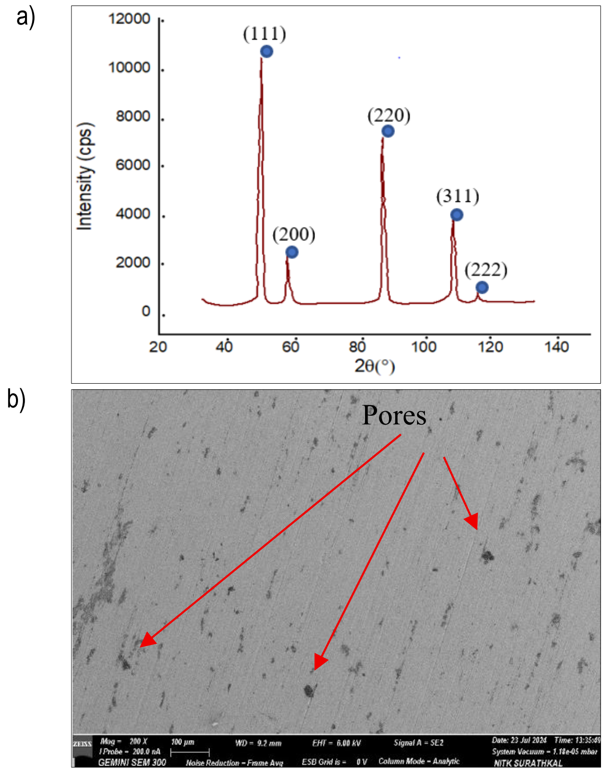

Fig. 2 (a) XRD pattern, (b) Microstructure of Invar 36

Tab. 1. Invar 36

Elements	S	Mo	P	C	Cr	Si	Mn	Ni	Fe
%	<0.003	<0.003	0.003	0.008	0.027	0.255	0.415	36.5	Balance

The cutting parameters for conducting the experiments have been selected using a 3-level design for the range of variables presented in Tab. 2. Turning was performed in a dry environment for all the experiments, and a single-pass experiment was carried out with a constant machining length of 60 mm. For this, the workpiece was divided into three sections, each measuring 60 mm, with each section being designated for a single machining pass. The tool and machine parameters are detailed in Tab. 2. The dry machining has been schematically represented in Fig. 3 (a), and the actual setup is presented in Fig. 3 (b).

DOI: 10.65731/ama/2026-0063

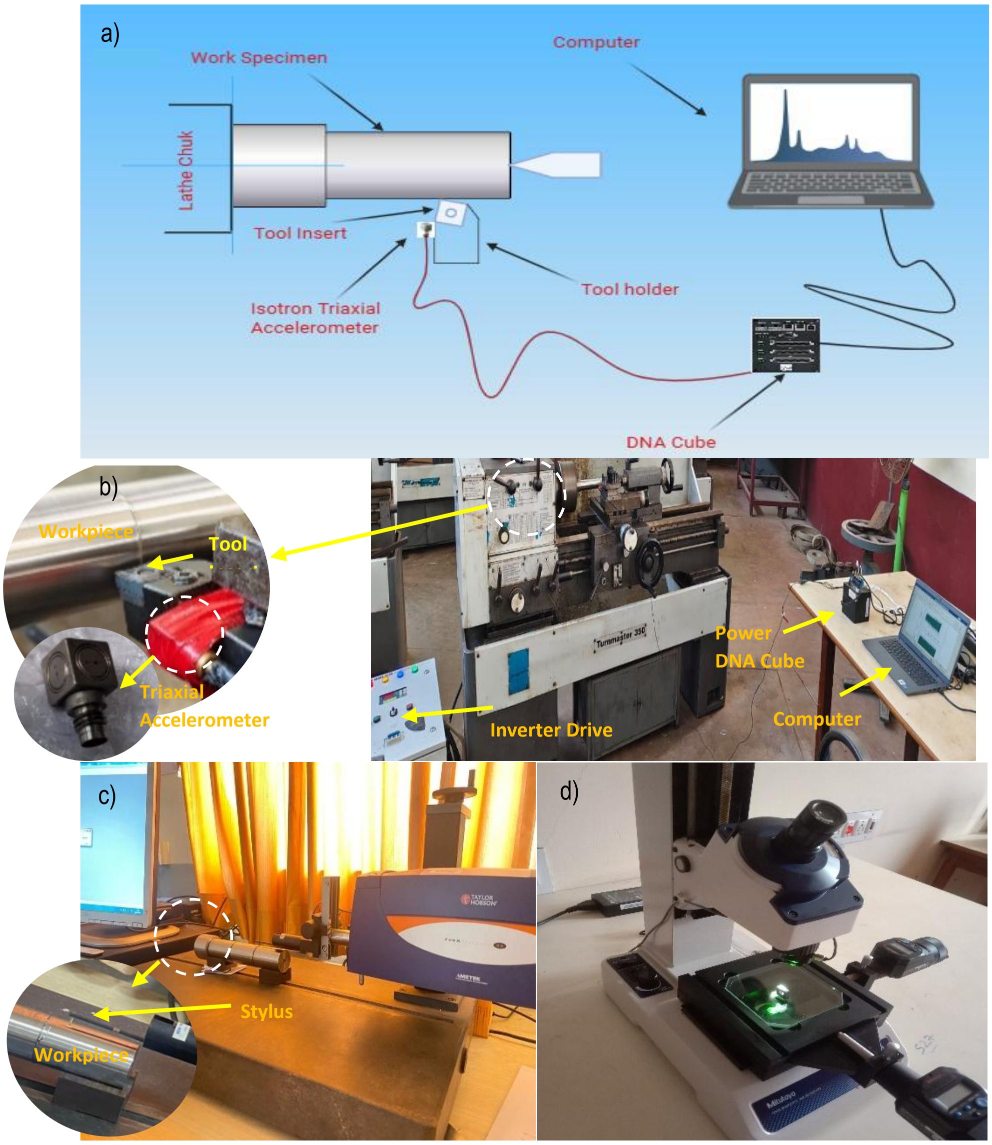

Fig. 3 (a) Schematic of the setup, (b) Actual setup, (c) Surface roughness testing, (d) Tool wear testing

Tab. 2. Machining conditions and parameters

Tool Holder and Insert	
Tool holder	PCLNR 2020 K12 (SECO make)
INSERT	CNMP 120408 K68- Uncoated (KENNAMETAL)
Process parameters	
v_c (m/min)	150, 175, 200
v_f (mm/rev)	0.18, 0.24, 0.28
a_p (mm)	0.8, 1.0, 1.2
Environment	Dry
Machining length (mm)	60 (Single pass)

Data regarding the key outputs, such as roughness, tool wear, and vibration, are collected. Measurements of vibration signals were carried out through a triaxial accelerometer in three perpendicular directions, which are radial (Vx), feed (Vy), and tangential (Vz). A Model 65-10 Isotron triaxial accelerometer was used to capture the signals coming from the vibrations in real time. The analog signals obtained from the experiment were transmitted to a DNA-PPCx at a high frequency of 10 kHz. The UEI Power DNA cube ensures a smooth acquisition and conversion of data. A computer with LabVIEW software was linked to this system, which is a storage of the high-frequency data produced during the machining process. The root mean square of the obtained signals was then calculated to facilitate the reading of the intensity of the signals. RMS analysis is a fundamental analysis of the intensity of the signals, while other variables, such as the peak amplitude, show the highest point of the signals. Microsoft Excel 2016 was used for the calculations. The formula applied for the RMS calculation is:

$$RMS = \sqrt{1/n \sum_{i=1}^{n} x_i^2} \tag{1}$$

where, n = is the total number of vibrations that are recorded in the selected steady state cutting period, x_i = vibration amplitude of the i[th] sample.

Further, a contact-type 2-D profilometer (TalySurf 50) was used to measure the roughness of the workpiece at three different locations along the circumference, spaced 120° apart. Measurements were taken using a sample length of 2.5 mm after each machining pass (Fig. 3 (c)). Additionally, as shown in Fig. 3 (d), the flank wear of the tool was inspected using a Tool Maker's Microscope (Mitutoyo) after each machining pass. The data obtained is analysed statistically with the help of Response Table Analysis. Many researchers [34-39] focused on the impact of process variables on output responses during machining operations have utilized Response Table Analysis to identify which process variable has the most significant effects on these outcomes.

2.2. Multi-criteria decision-making (MCDM) techniques optimization

For the determination of the optimal machining process parameters taking into account RMS vibration, flank wear, and surface roughness at the same time, three well-known MCDM methods such as GRA, ARAS, and EDAS were considered. As all criteria have to be minimized in the problem, the smaller-the-better approach has been used in the analysis.

2.2.1. Grey Relational Analysis (GRA)

Normalizing the measured values: the smaller-the-better criterion is expressed as:

$$y_i^*(k) = \left(\frac{max\, x_i^0(k) - x_i^0(k)}{max\, x_i^0(k) - min\, x_i^0(k)}\right) \tag{2}$$

Here, $x_i^0(k)$ =original value, i =tests, k =quality characteristic, and $y_i^*(k)$ =value after grey relation generation.

GRC:

$$\in_i(k) = \left(\frac{\Delta_{\min} - \zeta\Delta_{\max}}{\Delta_{0i}(k) - \zeta\Delta_{\max}}\right) \tag{3}$$

Here, $\Delta_{0i}(k)$ =offset in the absolute values between the reference $y_o^*(k)$ and comparability $y_i^*(k)$ sequence, ζ =distinguishing coefficient, Δ_{min} and $\Delta_{max}$are the least and highest of $\Delta_{0i}(k)$.

2.2.2. Grey Relational Grade (GRG)

$$\gamma_i = \frac{1}{n}\sum_{k=1}^{n} \in_i(k) \tag{4}$$

Here, γ_i =(0 to 1), and n =experiments.

Ranking: ranking is given based on the highest GRG values.

2.2.3. Additive Ratio Assessment (ARAS)

Decision making matrix:

$$X = \begin{pmatrix} x_{01} & x_{02} & \dots & x_{0n} \\ x_{11} & x_{12} & \dots & x_{1n} \\ . & . & . & . \\ x_{m1} & x_{m2} & \dots & x_{mn} \end{pmatrix}, \text{(i = 0, 1,.., m; j = 1, 2,.., n)},$$

$$x_{0j} = \begin{pmatrix} Max\, x_{ij} \;\; if\; j \in Beneficial \\ Min\, x_{ij} \;\; if\; j \in NonBeneficial \end{pmatrix} \tag{5}$$

Weighted normalized decision matrix:

$$x_{ij} = x_{ij}\, w_{ij}\;; i = 0, 1, \dots, m; \sum_{j=1}^{n} w_j = 1 \tag{6}$$

Optimality function:

$$S_j = \sum_{j=1}^{n} x_{ij}; \begin{pmatrix} i = 0, 1, \dots, m \\ j = 1, 2, \dots, n \end{pmatrix} \tag{7}$$

Degree of utility:

$$K_i = \frac{S_i}{S_o}; i = 0, 1, \dots, m \tag{8}$$

where, S_i and S_o are the optimality criterion values.

2.2.4. Distance from Average Solution (EDAS):

Average solution:

$$AS_j = \frac{\sum_{i=1}^{n} x_{ij}}{n} \tag{9}$$

Distance from average:

$$PDA_{ij} = \sum_{j=1}^{n} x_{ij}; \begin{pmatrix} \frac{max(0,(x_{ij} - AS_j))}{AS_j}\; if\; j \in Higher\ the\ better \\ \frac{max(0,(AS_j - x_{ij}))}{AS_j}\; if\; j \in Lower\ the\ better \end{pmatrix} \tag{10}$$

$$NDA_{ij} = \sum_{j=1}^{n} x_{ij}; \begin{pmatrix} \frac{max(0,(AS_j - x_{ij}))}{AS_j}\; if\; j \in Higher\ the\ better \\ \frac{max(0,(x_{ij} - AS_j))}{AS_j}\; if\; j \in Lower\ the\ better \end{pmatrix} \tag{11}$$

where, PDA_{ij} and NDA_{ij} denote the positive and negative distance of i[th] alternative from average solution in terms of j[th] criterion, respectively.

Appraisal score:

$$AS_i = \left[\frac{NSP_i + NSN_i}{2}\right] \tag{17}$$

A higher appraisal score shows better overall performance of the machining parameters. Here, all calculations and analysis involved in the MCDM methods were implemented with the use of MS Excel 2016 software.

3. RESULTS AND DISCUSSION

3.1. Experimental results

3.1.1 Influence of process parameters on RMS, VB_{max} and R_a

The results of the machining experiments are presented in Tab. 3.

Tab. 3. Results of the experiments

Exp. No.	v_c (m/min)	v_f (mm/rev)	a_p (mm)	RMS (V_x) (g)	VB_{max} (mm)	R_a (μm)
1	150	0.18	0.8	29.890	0.180	0.942
2	150	0.18	1.0	38.841	0.170	0.931
3	150	0.18	1.2	14.246	0.110	1.161
4	150	0.24	0.8	19.976	0.180	0.959
5	150	0.24	1.0	28.177	0.135	0.957
6	150	0.24	1.2	58.297	0.160	0.777
7	150	0.28	0.8	86.390	0.250	0.793
8	150	0.28	1.0	182.29	0.220	0.776
9	150	0.28	1.2	32.662	0.195	1.261
10	175	0.18	0.8	31.244	0.175	0.992
11	175	0.18	1.0	19.959	0.140	1.196
12	175	0.18	1.2	30.723	0.140	1.317
13	175	0.24	0.8	80.262	0.180	0.792
14	175	0.24	1.0	33.708	0.150	1.171
15	175	0.24	1.2	28.649	0.140	1.065
16	175	0.28	0.8	120.15	0.215	0.928
17	175	0.28	1.0	100.60	0.185	0.777
18	175	0.28	1.2	63.331	0.210	1.223
19	200	0.18	0.8	26.015	0.160	0.801
20	200	0.18	1.0	24.256	0.160	1.016
21	200	0.18	1.2	21.496	0.120	1.021
22	200	0.24	0.8	31.622	0.190	0.899
23	200	0.24	1.0	31.585	0.150	0.961
24	200	0.24	1.2	43.661	0.140	1.008
25	200	0.28	0.8	195.46	0.220	0.913
26	200	0.28	1.0	61.879	0.197	0.934
27	200	0.28	1.2	65.447	0.180	0.982

The vibration responses were recorded simultaneously along radial (V_x), axial (V_y), and tangential (V_z) directions during the dry turning process. Out of the above-mentioned vibration components, radial vibrations (V_x) play an especially significant role since this type of vibrations changes the instantaneous depth of cut, and as a consequence, the interaction of the tool and workpiece is affected. Changes in the effective depth of cut cause the changes in chip thickness, cutting forces, material separation mechanism, which are finally observed in the surface roughness. The radial vibrations have much more significant impact on surface roughness compared to the other two vibration components, axial and tangential, because radial vibration changes cutting geometry and surface generation mechanism. In addition, flank wear increases the contact length between tool and workpiece and causes force fluctuations and vibration amplification in radial direction. Thus, radial vibration is very sensitive to both the wear progression and deteriorated surface quality [40]. Vibration data analysis allows the understanding of the dynamic features of the machining process. Concentrating on time-domain signals, the researchers are able to see how machine vibrations change during machining [27]. With regard to the computation of RMS, the vibration signal was continuously collected during each of the machining trials. The RMS computations were done using the steady state cutting portion of the vibration signal recorded. The transient portions of the tool entering and exiting were not used in the computations since these portions had impact vibrations and not the actual cutting vibrations. Only the steady state cutting portion was used in computing the RMS. Time-domain signals of the vibration measured can be seen in the graphs in Fig. 4. The X-axis is time in milliseconds, and the Y-axis is acceleration amplitude in g. Figure 4 (a) shows the signal that corresponds to the minimum RMS vibration recorded, which was 14.246 g. The waveform has narrow fluctuations in amplitude of about ± 60 g. Conversely, the signal for the highest RMS vibration recorded is shown in Fig. 4 (b), captured at v_c=200 m/min, v_f=0.18 mm/rev, and a_p=1.2 mm. The acceleration here is far higher, showing wide fluctuations exceeding +150 g. The large difference between the vibration levels in the lowest (Fig. 4 (a)) and highest (Fig. 4 (b)) conditions clearly explains the variation in vibration levels because of various experimental conditions. Stable vibration levels ensure optimal machining conditions, improving the quality and stability of the machining process [41,42].

Tool wear parameter VB_{max} is a critical performance characteristic, with significant variation across the experiments observed in the present study. The lowest measured tool wear, 0.11 mm VB_{max} (Fig. 5 (a)), was obtained under the following cutting conditions: v_c=150 m/min, v_f=0.28 mm/rev, and a_p=0.8 mm. On the other hand, the highest tool wear of 0.25 mm VB_{max} (Fig. 5 (b)) was observed when the process variables were v_c=200 m/min, v_f=0.28 mm/rev, and a_p=0.8 mm.

The direct impact of process variables on workpiece machined surface is demonstrated by the two different machined surface roughness profiles shown in Fig. 6. For specific conditions of v_c=200 m/min, v_f=0.24 mm/rev, and a_p=0.8 mm, the surface having the smoothest profile is depicted in Fig. 6 (a) with the least magnitude consistent peak values. On the other hand, as shown in Fig. 6 (b), the roughest surface profile is produced at v_c =150 m/min, v_f =0.28 mm/rev, and a_p =1.0mm, with more noticeable peaks and valleys. These two profiles (Fig. 6 (a) and (b)) are compared to emphasize the different surface finishes that are able to be achieved through machining operations. Their significance lies in drawing attention to the importance of determining specific combinations in ensuring final surface quality during machining.

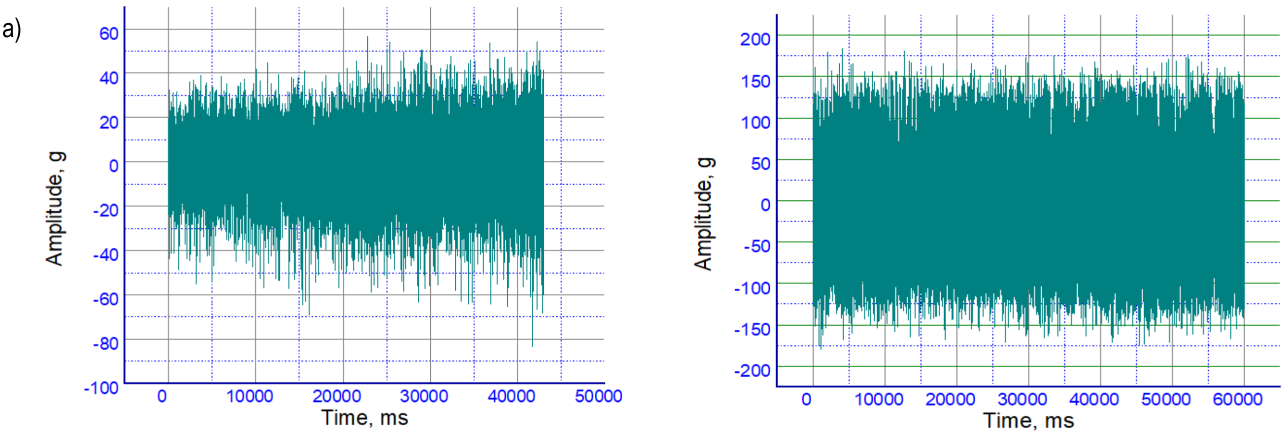

Fig. 4 Time domain vibrational signal at (a) lowest measured RMS and (b) highest measured RMS

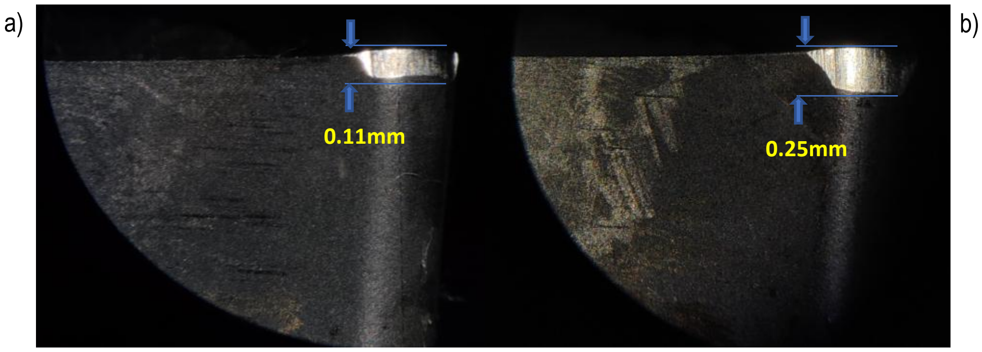

Fig. 5 Tool Flank wear (a) Lowest VB_{max}, (b) Highest VB_{max}

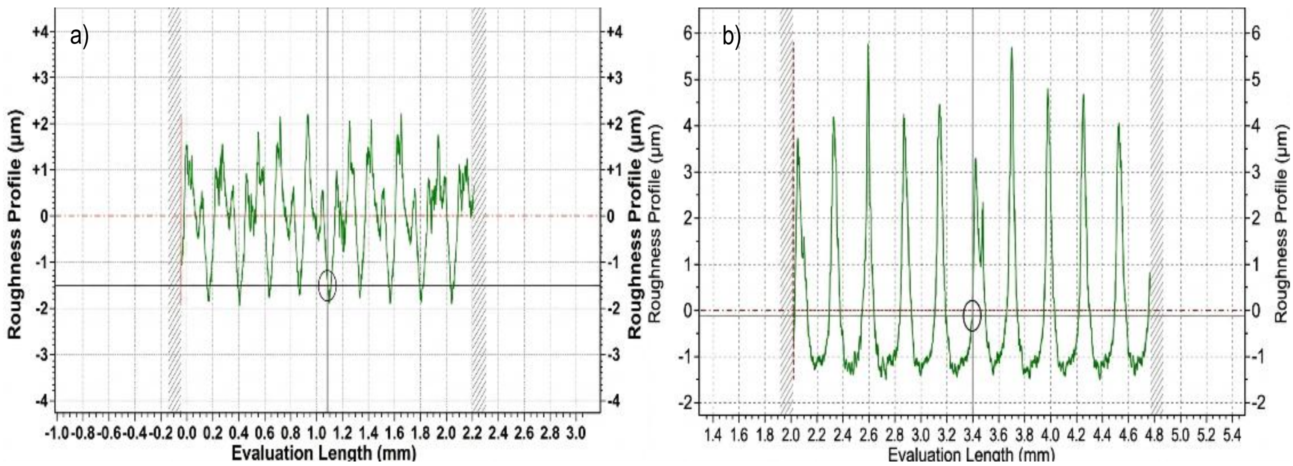

Fig. 6 Profile of machined surface roughness (a) smoothest, (b) roughest

3.3.1. Response table analysis and main effects plots

Response Table Analysis results for the effect of process variables on RMS, VB_{max}, and R_a are shown in Fig. 7 and Table 4. According to the analysis, cutting speed is the most influential parameter in relation to both RMS vibration and VB_{max}, while the feed rate parameter is the most influential in relation to Ra. In regard to RMS vibration, cutting speed had the highest Delta value since cutting speed differences caused the most significant change in vibration amplitude. During dry turning process, increasing cutting speed causes higher temperatures, frictional interaction, and dynamic load at the interface of the tool and workpiece, leading to vibrations [43]. The feed rate was the second most influential parameter because the higher the feed rate, the higher the chip load and the cutting force, leading to higher vibration values, while the depth of cut is the least influential parameter. Similarly, the greatest change (Delta value) in VB_{max} was recorded with increasing cutting speed. The main reason behind the significant effect of cutting speed is the high thermal and tribological loading

DOI: 10.65731/ama/2026-0063

on the cutting edge. Several researchers have found that increased cutting speeds cause the processes of adhesion, abrasion, and wear due to the high temperature levels developed during machining difficult-to-machine nickel-based alloys [44]. Moreover, the reason behind the limited thermal conductivity and adhesion properties results in low heat dissipation from the cutting area leading to flank wear formation. Increased mechanical loading of the cutting edge is another reason behind the effect of feed rate on the process of wear [41]. With regard to surface roughness, the feed rate was found to be the predominant influencing factor. Some researchers have indicated that this is in accordance with the basics of turning operations, since the feed rate determines the distance and height of the feed marks that are produced on the surface. The surface profile height increases theoretically with an increase in feed rate; thus, there is an impact on the quality of the surface finish. There is a direct influence of the vibration characteristics between the tool and work piece in determining the topography of the surface during turning operations. Hence, even though vibration affects the surface, the feed rate is the primary factor for determining the surface roughness. Depth of cut followed feed rate as it affects vibrations and cutting force [40]. The RMS (Root Mean Square) vibration value is often used in the machining process to evaluate the state of the tool due to the fact that vibration energy normally grows while the tool wears out. A comparison of Fig. 7(a) and Fig. 7(b) reveals a certain connection between RMS vibration and VB_{max} under the studied cutting conditions. Increased flank wear tends to result in higher vibration values, whereas lower flank wear is related to smaller vibration amplitudes [44]. Such results may be explained by the higher friction coefficient at the interface between the tool and the chip, irregularity of chip formation, reduced sharpness of the cutting edge, increased cutting forces, and dynamic instability created by the worn cutting edge. All these factors contribute to higher vibration amplitude and vibration energy, consequently increasing the RMS value [45,46].

However, it has been noted that the response of surface roughness was different from the response of tool wear. Generally speaking, the increase in tool wear results in an increase in surface roughness during the machining process. However, sometimes surface roughness decreases in spite of an increase in tool wear. As a result, a slight burnishing effect appears on the surface of the workpiece, which makes the surface better in spite of the wear that exists. Such situations were also observed during the machining of difficult materials, like titanium [28]. Hence, even though the excessive tool wear leads to a worse surface, the moderate wear can make the surface better.

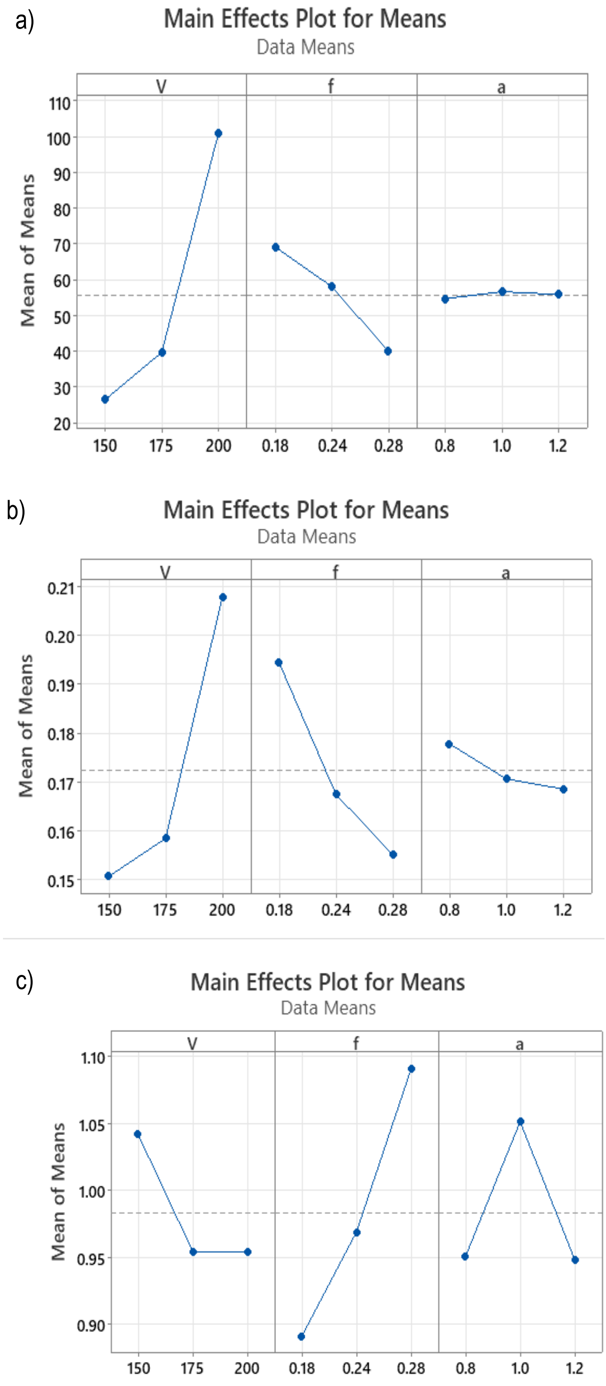

Fig. 7 Main Effects Plots- Behaviour of (a) RMS, (b) VB_{max}, (c) R_a with respect to process parameters

Tab 4. Response Table for RMS, VB_{max}, and R_a

	RMS (g)			VB_{max} (mm)			R_a (μm)		
Level	v_c (m/min)	v_f (mm/rev)	a_p (mm)	v_c (m/min)	v_f (mm/rev)	a_p (mm)	v_c (m/min)	v_f (mm/rev)	a_p (mm)
1	26.30	69.00	54.53	0.1506	0.1944	0.1778	1.0418	0.8910	0.9507
2	39.55	57.92	56.51	0.1583	0.1674	0.1706	0.9544	0.9687	1.0513
3	100.91	39.83	55.71	0.2079	0.1550	0.1685	0.9541	1.0904	0.9482
Delta	74.62	29.17	1.98	0.0574	0.0394	0.0093	0.0877	0.1994	0.1030
Rank	1	2	3	1	2	3	3	1	2

3.2. Optimization results

3.2.1. Grey Relational Analysis (GRA)

Tab. 5. shows the implementation of GRA for optimizing the responses R_a, VB_{max}, and RMS values. First, weightage is allotted equally with the value of 0.33 for surface roughness (R_a), tool wear (VB_{max}), and vibration (RMS). The experimental results are normalized (normalized R_a, VB_{max}, RMS) in such a way that all responses vary between 0 and 1, where 1 is the optimal response for all. The Deviation Sequence is obtained by finding the deviation between the normalized response and optimal response (1), followed by calculating the Grey Relational Coefficient (GRC) for all responses. The Grey Relational Grade (GRG), or overall response measure, is an average value of GRC. ranks have been allotted based on the highest to lowest GRG values. From the GRA method, the Exp. No. 3 (v_c = 150 m/min, v_f = 0.18 mm/rev, a_p = 1.2 mm) is ranked first with GRG value of 0.772.

Tab. 5. Results of Grey Relational Analysis (GRA)

Exp No.	R_a (µm)	VB_{max} (mm)	RMS (g)	R_a (µm)	VB_{max} (mm)	RMS (g)	R_a (µm)	VB_{max} (mm)	RMS (g)	GRG	RANK
	Normalised			Deviational Sequence			GRC				
1	0.693	0.500	0.914	0.307	0.500	0.086	0.518	0.398	0.793	0.569	15
2	0.713	0.571	0.864	0.287	0.429	0.136	0.535	0.435	0.709	0.560	16
3	0.289	1.000	1.000	0.711	0.000	0.000	0.317	1.000	1.000	0.772	1
4	0.661	0.500	0.968	0.339	0.500	0.032	0.493	0.398	0.913	0.601	7
5	0.666	0.821	0.923	0.334	0.179	0.077	0.497	0.649	0.811	0.652	5
6	0.998	0.643	0.757	0.002	0.357	0.243	0.993	0.480	0.576	0.683	4
7	0.968	0.000	0.602	0.032	1.000	0.398	0.912	0.248	0.453	0.538	19
8	1.000	0.214	0.073	0.000	0.786	0.927	1.000	0.296	0.262	0.519	21
9	0.104	0.393	0.898	0.896	0.607	0.102	0.269	0.352	0.765	0.462	24
10	0.600	0.536	0.906	0.400	0.464	0.094	0.452	0.415	0.779	0.549	17
11	0.224	0.786	0.968	0.776	0.214	0.032	0.298	0.606	0.913	0.606	6
12	0.000	0.786	0.909	1.000	0.214	0.091	0.248	0.606	0.784	0.546	18
13	0.971	0.500	0.636	0.029	0.500	0.364	0.918	0.398	0.475	0.597	10
14	0.270	0.714	0.893	0.730	0.286	0.107	0.311	0.536	0.754	0.534	20
15	0.465	0.786	0.921	0.535	0.214	0.079	0.382	0.606	0.806	0.598	9
16	0.718	0.250	0.416	0.282	0.750	0.584	0.540	0.306	0.361	0.402	25
17	0.997	0.464	0.523	0.003	0.536	0.477	0.991	0.381	0.409	0.594	11
18	0.174	0.286	0.729	0.826	0.714	0.271	0.285	0.316	0.549	0.384	26
19	0.954	0.643	0.935	0.046	0.357	0.065	0.877	0.480	0.836	0.731	2
20	0.556	0.643	0.945	0.444	0.357	0.055	0.426	0.480	0.857	0.588	12
21	0.548	0.929	0.960	0.452	0.071	0.040	0.422	0.822	0.892	0.712	3
22	0.772	0.429	0.904	0.228	0.571	0.096	0.591	0.366	0.775	0.577	13
23	0.658	0.714	0.904	0.342	0.286	0.096	0.491	0.536	0.775	0.601	8
24	0.571	0.786	0.838	0.429	0.214	0.162	0.435	0.606	0.670	0.570	14
25	0.747	0.214	0.000	0.253	0.786	1.000	0.566	0.296	0.248	0.370	27
26	0.708	0.382	0.737	0.292	0.618	0.263	0.530	0.348	0.557	0.478	22
27	0.620	0.500	0.717	0.380	0.500	0.283	0.465	0.398	0.539	0.467	23

3.2.2. Additive Ratio Assessment (ARAS)

Tab. 6. illustrates the results of the ARAS method applied to data obtained from the experiments. Positive and negative distances from the average solution are identified based on whether the criterion is helpful or unhelpful. Normalization is the initial step that is subjected to output responses, namely R_a, VB_{max}, and RMS. The resulting values are then multiplied by the weight corresponding to the criteria to get the values under the columns of the Weighted Decision Matrix for R_a, VB_{max}, and RMS. These weighted values are the relative importance of each response to an experiment. Here, 0.33 is the weight assigned to each output response. Further, the method involves calculating the appraisal score and utility degree (K_i) to rank the experiments. The condition with the highest utility degree value is assigned Rank 1. The final ranking showed that the optimal experimental condition reached the highest K_i value of 0.920. This top-ranked experiment is Exp. No. 3 corresponds to v_c =150 m/min, v_f =0.18 mm/rev, a_p =1.2 mm.

DOI: 10.65731/ama/2026-0063

Tab. 6. Results of Additive Ratio Assessment (ARAS)

Exp No.	R_a (μm)	VB_{max} (mm)	RMS (g)	R_a (μm)	VB_{max} (mm)	RMS (g)	Optimality function (S_i)	Utility degree (K_i)	RANK
	Normalized			Weighted Normalized					
1	0.036	0.032	0.041	0.012	0.011	0.013	0.036	0.599	10
2	0.037	0.034	0.031	0.012	0.011	0.010	0.034	0.561	16
3	0.029	0.053	0.085	0.010	0.017	0.028	0.055	0.920	1
4	0.035	0.032	0.061	0.012	0.011	0.020	0.042	0.707	4
5	0.036	0.043	0.043	0.012	0.014	0.014	0.040	0.669	6
6	0.044	0.036	0.021	0.014	0.012	0.007	0.033	0.555	17
7	0.043	0.023	0.014	0.014	0.008	0.005	0.026	0.441	23
8	0.044	0.026	0.007	0.014	0.009	0.002	0.025	0.423	24
9	0.027	0.030	0.037	0.009	0.010	0.012	0.031	0.517	18
10	0.034	0.033	0.039	0.011	0.011	0.013	0.035	0.585	13
11	0.028	0.042	0.061	0.009	0.014	0.020	0.043	0.719	3
12	0.026	0.042	0.039	0.009	0.014	0.013	0.035	0.588	11
13	0.043	0.032	0.015	0.014	0.011	0.005	0.030	0.497	19
14	0.029	0.039	0.036	0.010	0.013	0.012	0.034	0.571	14
15	0.032	0.042	0.042	0.011	0.014	0.014	0.038	0.637	8
16	0.037	0.027	0.010	0.012	0.009	0.003	0.024	0.406	26
17	0.044	0.031	0.012	0.014	0.010	0.004	0.029	0.480	20
18	0.028	0.028	0.019	0.009	0.009	0.006	0.025	0.411	25
19	0.042	0.036	0.047	0.014	0.012	0.015	0.041	0.690	5
20	0.033	0.036	0.050	0.011	0.012	0.016	0.040	0.659	7
21	0.033	0.049	0.056	0.011	0.016	0.019	0.046	0.760	2
22	0.038	0.031	0.038	0.012	0.010	0.013	0.035	0.587	12
23	0.035	0.039	0.038	0.012	0.013	0.013	0.037	0.619	9
24	0.034	0.042	0.028	0.011	0.014	0.009	0.034	0.567	15
25	0.037	0.026	0.006	0.012	0.009	0.002	0.023	0.385	27
26	0.036	0.030	0.020	0.012	0.010	0.006	0.028	0.471	21
27	0.035	0.032	0.019	0.011	0.011	0.006	0.028	0.470	22

3.2.3. Distance from Average Solution (EDAS)

Tab. 7. illustrates the results of the EDAS method applied to data from the machining experiments. First, the average value of each criterion was calculated and treated as the reference solution. Based on this reference, the PDA and NDA values are calculated for each experimental value. These values are multiplied by respective normalised weights to obtain the weighted positive and negative distances. The summation of weighted PDA values results in the Positive Score (SP), while the summation of weighted NDA values yields the negative score (SN). SP and SN were normalised to obtain the Normalised Positive Score (NSP) and Normalised Negative Score (NSN). The Appraisal Score Index was then calculated using the normalised scores to represent the overall performance of each experiment. The experiments were ranked based on their Appraisal Score Index (ASI) values, where a higher ASI indicates better performance. The highest ASI value of 0.968 was obtained for Exp No. 3, indicating optimal turning condition among all 27 experimental conditions. This top-ranked experimental condition corresponds to v_c =150 m/min, v_f =0.18 mm/rev, a_p =1.2 mm.

Tab. 7. Results of Distance from Average Solution (EDAS)

Exp No.	Weighted Sum of PDA			Weighted Sum of NDA			NSNI	ASI	RANK
	R_a (μm)	VB_{max} (mm)	RMS (g)	R_a (μm)	VB_{max} (mm)	RMS (g)			
1	0.014	0.000	0.153	0.000	0.015	0.000	0.984	0.720	11
2	0.018	0.004	0.099	0.000	0.000	0.000	1.000	0.666	16
3	0.000	0.119	0.245	0.059	0.000	0.000	0.935	0.968	1
4	0.008	0.000	0.211	0.000	0.015	0.000	0.984	0.793	6
5	0.009	0.071	0.163	0.000	0.000	0.000	1.000	0.833	5
6	0.069	0.024	0.000	0.000	0.000	0.016	0.983	0.618	17
7	0.064	0.000	0.000	0.000	0.149	0.183	0.640	0.408	23
8	0.070	0.000	0.000	0.000	0.091	0.752	0.085	0.138	26
9	0.000	0.000	0.136	0.093	0.044	0.000	0.852	0.612	18
10	0.000	0.000	0.145	0.003	0.005	0.000	0.991	0.694	14
11	0.000	0.062	0.212	0.071	0.000	0.000	0.923	0.836	4

12	0.000	0.062	0.148	0.112	0.000	0.000	0.879	0.726	10
13	0.064	0.000	0.000	0.000	0.015	0.146	0.825	0.501	19
14	0.000	0.043	0.130	0.063	0.000	0.000	0.932	0.702	13
15	0.000	0.062	0.160	0.027	0.000	0.000	0.970	0.789	7
16	0.019	0.000	0.000	0.000	0.082	0.383	0.495	0.273	25
17	0.069	0.000	0.000	0.000	0.024	0.267	0.684	0.437	22
18	0.000	0.000	0.000	0.080	0.072	0.046	0.785	0.392	24
19	0.061	0.024	0.176	0.000	0.000	0.000	1.000	0.857	3
20	0.000	0.024	0.186	0.011	0.000	0.000	0.988	0.781	8
21	0.000	0.100	0.202	0.012	0.000	0.000	0.986	0.908	2
22	0.028	0.000	0.142	0.000	0.034	0.000	0.963	0.715	12
23	0.008	0.043	0.142	0.000	0.000	0.000	1.000	0.764	9
24	0.000	0.062	0.071	0.008	0.000	0.000	0.991	0.677	15
25	0.024	0.000	0.000	0.000	0.091	0.830	0.000	0.033	27
26	0.017	0.000	0.000	0.000	0.046	0.037	0.909	0.477	20
27	0.001	0.000	0.000	0.000	0.015	0.059	0.920	0.461	21

The rankings calculated based on GRA, EDAS, and ARAS showed that Experiment 3 (v_c = 150 m/min, v_f = 0.18 mm/rev, a_p = 1.2 mm) was the optimal process condition for machining operation. While Experiment 3 did not show the lowest surface roughness value, it produced the lowest vibration (RMS = 14.246 g) and lowest flank wear (VB_{max} = 0.110 mm) values. Considering that multi-criteria optimization looks for the best compromise solution with respect to conflicting criteria, the overall high performance of Experiment 3 gave it the top position in the ranking. From the viewpoint of the machining operation, a low cutting speed decreased the frictional heat and temperature at the tool-chip interface and slowed down wear formation and ensured cutting edge integrity. Such behaviour has been observed in machining of hard-to-cut alloys when cutting speed increases and wear formation gets faster due to the increase in thermal and tribological aspects [43-46]. A low feed rate (0.18 mm/rev) led to a decrease in the chip load and force fluctuation, ensuring dynamic stability and low vibration level. Earlier investigations have proved that low vibration amplitudes ensure higher machining stability and prevent the excessive wear of the cutting tool and machined surface [47–52]. While the minimum surface roughness was attained under varying machining conditions, Experiment 3 was found to have the lowest vibration and tool wear values at the same time. However, because multi-criteria optimization involves obtaining the optimal compromise among the performance metrics rather than obtaining the optimal value of one response alone, the combined performance of RMS vibration and VB_{max} overcame the slight increase in surface roughness to give Experiment 3. This is in accordance with the suggested mechanistic feedback-loop model which states that tool wear, vibration and surface quality develop in an interrelated manner and hence should not be considered in isolation [47-52].

The consistent selection of experiment 3 by GRA, EDAS and ARAS shows that the process of optimization was very successful and confirms that the stable machining conditions characterized by low vibration and low tool wear yield the best machining performance in the case of dry turning of Invar 36.

3.2. Vibration Analysis using Fast Fourier Transform (FFT) of Machining Stability

3.2.1. FFT Analysis – V_x Radial for Experiment 3

The V_x (radial vibration signal) obtained in Experiment 3 consists of three phases as can be seen in Fig. 8(a), a phase with low vibration level at the time of tool engagement (0-0.9 s), the phase where vibrations stabilize after the stabilization of the cutting process (0.9 to 9.0 s), and a phase with rapid drop in vibration levels in case of tool withdrawal. In order to reduce the effect of transients due to tool entry/withdrawal, the window from 4.60 s to 8.90 s was considered for the frequency domain analysis. As depicted in Fig. 8(b), the FFT spectrum obtained till the Nyquist frequency of 5000 Hz shows a broadband cluster of resonances ranging from about 4000 to 4300 Hz which appears to be related to machine–tool–toolholder structural resonances [47,48]. The analysis of the frequency band pertaining to machining presented in Fig. 8(c) reveals the existence of a prominent peak at around 105.6 Hz, showing that there exists an accumulation of vibration energy at a particular frequency related to the machining process. Other peaks of low amplitude have been identified around 14 Hz and 27 Hz and the expanded low frequency spectrum of Fig. 8(d) illustrates that there exists a harmonics relationship associated with the dynamic performance of the machine-tool and the low frequency vibrations of the structure [49,50]. In contrast to the highly dynamic unstable state represented by Experiment 25, there exist only low amplitudes and no dominant peaks with high amplitudes within the machining frequency range. The relatively low value of RMS of 14.246 indicates the stability of the cutting process and implies that the vibration amplitude level is tolerable for this optimum machining state [51,52].

 DOI: 10.65731/ama/2026-0063

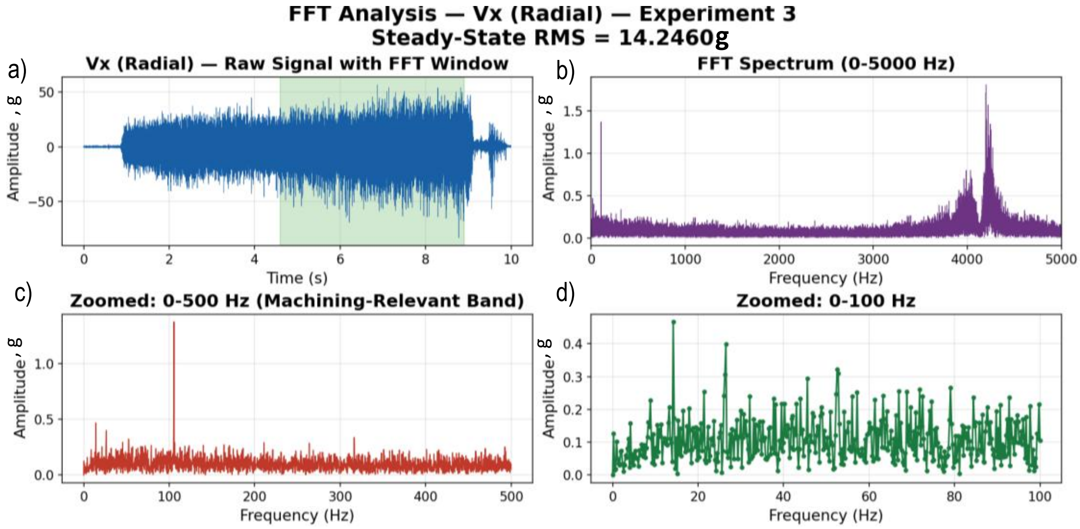

Fig. 8. FFT analysis of radial vibration (Vx) for Experiment 3 (v_c = 150 m/min, v_f = 0.18 mm/rev, a_p = 1.2 mm), indicating that there is stable cutting behavior with a predominant frequency of 105.6 Hz

3.2.2. FFT Analysis – V_x Radial for Experiment 25

The FFT analysis of the signal of radial vibration (Vx) obtained from Experiment 25 (v_c=200 m/min; v_f = 0.28 mm/rev; a_p = 0.8 mm) is illustrated in Fig. 9. As can be seen from Fig. 8(a), the signal in time domain has severe dynamic excitation and vibration amplitude reaches the data acquisition limits of ±250 mV during steady state cutting process. Furthermore, this is also indicated by the signal during steady state cutting process in Fig. 9(b) and extremely high value of RMS of 193.07 g. As indicated in the FFT spectrum presented in Fig. 9(c), there exists a high peak of the frequency at around 2311.6 Hz with several other nearby frequency peaks. Generally, the existence of a high peak at a particular high frequency is an indication of structural resonance induced dynamic instability in machining processes, especially where the excitation frequency is close to one of the natural frequencies of the machine-tool-workpiece system [47,48]. The machining-related frequency band depicted in Fig. 9(d) includes small-amplitude components alone, while the fine low-frequency spectrum of Fig. 9(e) shows a small peak close to 20 Hz, which could possibly represent the contribution due to spindle rotation and its harmonics. Such low-frequency components are very common during turning and are usually related to the contribution of spindle rotation, imbalance, or machine-tool dynamics instead of being induced by chatter vibrations [51]. This significant difference between low-frequency operational components and the strong peak of 2311.6 Hz implies that the vibration behavior is mainly determined by the high-frequency structural excitation [52].Therefore, the FFT analysis results clearly indicate the existence of dynamic instability during the above machining condition and explain the reason behind the large RMS vibration value, increased flank wear, and poor surface quality that result from these higher machining parameters. Some studies in the past have suggested that high vibration and chatter lead to high cutting dynamic forces, rapid tool wear, and poor surface topography [47-52].

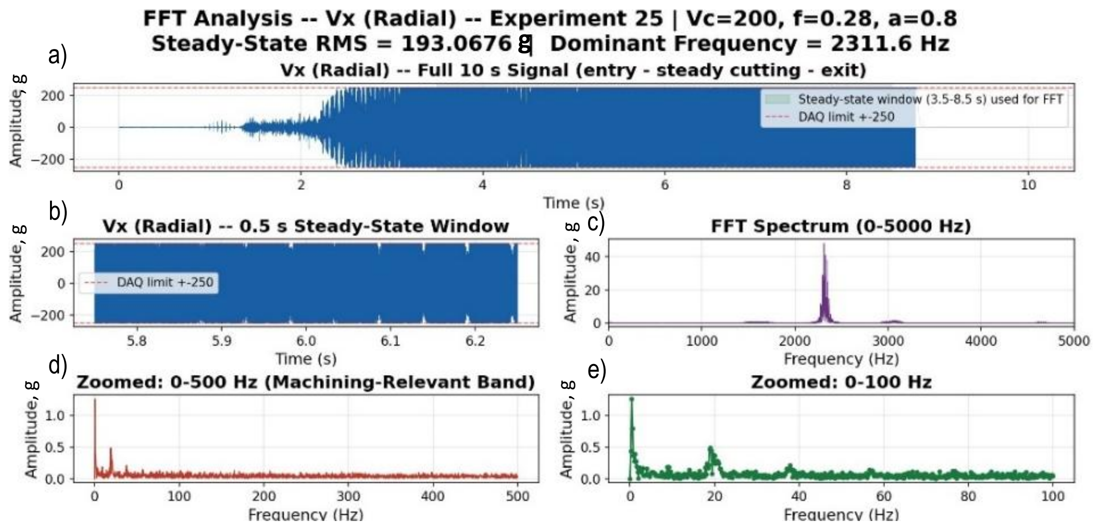

Fig. 9. FFT analysis of radial vibration (Vx) for Experiment 3 (v_c = 150 m/min, v_f = 0.18 mm/rev, a_p= 1.2 mm), indicating that there is stable cutting behavior with a predominant frequency of 105.6 Hz

3.3. Mechanistic relationship between tool wear, vibration (RMS) and surface roughness

Figure 10 shows the closed feedback loop relationship among tool wear (VB_{max}), vibration (RMS) and surface roughness (R_a) in dry turning operation of Invar 36. The characteristics of Invar 36 such as low thermal conductivity, high ductility and adhesiveness result in increased heat generation in the cutting area, and hence the tool is prone to wear [43]. Besides, the chosen machining parameters such as cutting speed, feed rate and depth of cut affect the wear rate on the flank of the tool during machining. With the increasing flank wear, there will be a change in the cutting geometry which causes an increase in the friction at the tool-chip interface and at the tool-workpiece interface. The variation in cutting forces causes instability and increase in vibration amplitude, thus causing the rise in RMS values. Such relationship has been found in machining research for difficult-to-machine alloys [44-46,51]. This can be expressed using Mechanism 1, shown in Fig. 10. In Mechanism 2, there will be an increase in vibration produced during the process of cutting and transfer this vibration to the machined surface. Oscillations cause the formation of surface waviness, chatter marks, and geometrical deviations, thus increasing the arithmetic mean surface roughness. The vibrations of the tool and workpiece cause topography production, whereas there are other machining dynamics research showing the contribution of vibration instability to surface quality deterioration [47-52]. As the machined surface becomes rough, the cutting operation faces increasingly uneven contact conditions between the tool and the workpiece. The increased friction and abrasion thus lead to more flank wear formation and further damage to the cutting edge [43-46]. This wear mechanism is depicted in Fig. 10 by Mechanism 3. As a result, a positive feedback system will be generated where tool wear causes vibration, vibration leads to surface roughness, and surface roughness causes tool wear. From the above mechanical model, one can find the physical reason behind the results experimentally found in this study for the relationship between the VB_{max}, RMS vibrations, and surface roughness of Invar 36. The proposed feedback loop model helps to explain the relationship between VB_{max}, RMS vibration, and surface roughness from an experimental perspective. The study shows that tool wear, vibration formation, and surface damage occur at the same time through mutual physical phenomena, which is supported by earlier investigations reporting close relationships between tool wear, vibrations, dynamic stability, and surface integrity during machining processes [51,52].

Fig. 10. Mechanistic feedback-loop illustrating the interrelationship among tool wear (VB_{max}), machining vibration (RMS), and surface roughness (R_a) during dry turning of Invar 36

4. CONCLUSIONS

Nickel-based alloys, especially INVAR 36, is a trending material in the research community. The present study explored the performance of the tool and alloy during the high-speed machining of this alloy. For the range of process input variables that are tested in the present study, the observations and conclusions can be drawn as follows –

- The most significant parameter that affects both RMS vibration and VB_{max} is the cutting speed, while the feed rate has the maximum effect on R_a.
- Optimum RMS vibration (14.246 g) and VB_{max} (0.110 mm) were achieved in Experiment 3 (v_c = 150 m/min, v_f = 0.18 mm/rev, a_p = 1.2 mm), which means good machining stability and tool performance.
- Surface roughness depends mainly on the feed rate, and the low values of the feed rate provide high surface finish since there will be no feed marks generated on the surface.
- The optimum vibration frequency showed the concentration of energy vibration in the narrow band of low-frequency range, which is an indication of stable cutting and lack of dynamic instability.

- Experiment 25 (v_c = 200 m/min, v_f = 0.28 mm/rev, a_p = 0.8 mm) had the highest RMS vibration (193.07 g) and dominated the frequency at 2311.6 Hz.
- The vibration and tool wear responses demonstrated almost identical behavior over the machining range under investigation, validating a high level of relationship between flank wear and vibration during dry machining of Invar 36.
- Experiment 3 was found to be the best machining parameter by GRA, ARAS, and EDAS criteria, ensuring the effectiveness of the employed MCDM methods in the multi-criteria optimization of vibration, tool wear, and surface roughness.

Further research will be conducted in areas related to RSM-based predictive models, regression analysis, interaction effect investigation, formulation of energy-based machining model, and characterization of chatter via machine-tool dynamic stability analysis.

REFERENCES

1. Yonezawa T. Nickel alloys: Properties and characteristics. In: Comprehensive Nuclear Materials. Elsevier; 2012. p. 233–66.
2. Shetty SM, Marakini V, Mello G, Pai SP, Dsouza EW, Dsouza LA, et al. Comparative Analysis of Surface Roughness and Tool Wear under Dry, MQL, and Cryogenic Machining Conditions in Invar 36 Turning Operations. Journal of Mines Metals and Fuels. 2025. Available from: https://doi.org/10.18311/jmmf/2025/47546.
3. Pedroso AFV, Sebbe NPV, Costa RDFS, Barbosa MLS, Sales-Contini RCM, Silva FJG, et al. INCONEL® alloy machining and Tool Wear Finite Element Analysis assessment: An extended review. J Manuf Mater Process [Internet]. 2024;8(1):37. Available from: http://dx.doi.org/10.3390/jmmp8010037
4. Sousa VFC, Fernandes F, Silva FJG, Costa RDFS, Sebbe N, Sales-Contini RCM. Wear behavior phenomena of TiN/TiAlN HiPIMS PVD-coated tools on milling Inconel 718. Metals (Basel) [Internet]. 2023;13(4):684. Available from: http://dx.doi.org/10.3390/met13040684
5. Martinho RP, Silva FJG, Martins C, Lopes H. Comparative study of PVD and CVD cutting tools performance in milling of duplex stainless steel. Int J Adv Manuf Technol [Internet]. 2019;102(5–8):2423–39. Available from: http://dx.doi.org/10.1007/s00170-019-03351-8
6. Altintas Y. Manufacturing automation: Metal cutting mechanics, machine tool vibrations, and CNC design [Internet]. 2nd ed. Cambridge, England: Cambridge University Press; 2012. Available from: http://dx.doi.org/10.1017/cbo9780511843723
7. Huang G, He G, Gong X, He Y, Liu Y, Huang K. Additive manufacturing of Invar 36 alloy. J Mater Res Technol [Internet]. 2024;30:1241–68. Available from: http://dx.doi.org/10.1016/j.jmrt.2024.02.221
8. Eissel A, Engelking L, Gustus R, Treutler K, Wesling V, Schroepfer D, et al. Alloy modification for additive manufactured Ni alloy components—part I: effect on microstructure and hardness of Invar alloy. Weld World [Internet]. 2023;67(4):1049–57. Available from: http://dx.doi.org/10.1007/s40194-023-01510-w
9. Khanna N, Mistry S, Rahman Rashid RA, Gupta MK. Investigations on density and surface roughness characteristics during selective laser sintering of Invar-36 alloy. Mater Res Express [Internet]. 2019;6(8):086541. Available from: http://dx.doi.org/10.1088/2053-1591/ab18bd
10. Yakout M, Phillips I, Elbestawi MA, Fang Q. In-situ monitoring and detection of spatter agglomeration and delamination during laser-based powder bed fusion of Invar 36. Opt Laser Technol [Internet]. 2021;136(106741):106741. Available from: http://dx.doi.org/10.1016/j.optlastec.2020.106741
11. Huang G, He G, Peng X, He Y, Chen H, Huang K, et al. Effect of processing parameters on the microstructure, mechanical properties and thermal expansion behavior of Invar 36 alloy manufactured by laser powder bed fusion. Mater Sci Eng A Struct Mater [Internet]. 2024;897(146329):146329. Available from: http://dx.doi.org/10.1016/j.msea.2024.146329
12. Nguyen N-T, Nguyen A-T, Nguyen T-S, Le N-T. Using VIKOR and RSM-DA in the optimization of dry turning of 9XC steel. Istraz Proj Za Privredu [Internet]. 2024;22(2):10–8. Available from: http://dx.doi.org/10.5937/jaes0-43392
13. Deppermann M, Puls H, Burghold M, Kneer R, Klocke F. Experimental investigation of the work piece temperatures in dry orthogonal metal turning. In: Proceedings of the 15th International Heat Transfer Conference. Connecticut: Begellhouse; 2014.
14. Korpysa J, Kuczmaszewski J, Zagórski I. Surface quality of AZ91D magnesium alloy after precision milling with coated tools. Strojniski Vestn [Internet]. 2023;69(11–12):497–508. Available from: http://dx.doi.org/10.5545/sv-jme.2023.651
15. Ghazali MHM, Mazlan AZA, Wei LM, Tying CT, Sze TS, Jamil NIM. Effect of machining parameters on the surface roughness for different type of materials. IOP Conf Ser Mater Sci Eng [Internet]. 2019;530(1):012008. Available from: http://dx.doi.org/10.1088/1757-899x/530/1/012008
16. Evgeny B, Hughes T, Eskin D. Effect of surface roughness on corrosion behaviour of low carbon steel in inhibited 4 M hydrochloric acid under laminar and turbulent flow conditions. Corros Sci [Internet]. 2016;103:196–205. Available from: http://dx.doi.org/10.1016/j.corsci.2015.11.019
17. Zhang J, Li R, Zhang L, Yang H, Tang H, Chen S. On the tool wear mechanism of machining Zr-based bulk metallic glasses under varying corner radii. J Non Cryst Solids [Internet]. 2024;624(122722):122722. Available from: http://dx.doi.org/10.1016/j.jnoncrysol.2023.122722
18. Arslan H, Osman Er A, Orhan S, Aslan E. Tool condition monitoring in turning using statistical parameters of vibration signal. Int J Acoust Vib [Internet]. 2016;21(4). Available from: http://dx.doi.org/10.20855/ijav.2016.21.4432
19. Serra R, Rmili W. Experimental evaluation of flank wear in dry turning from accelerometer data. Int J Acoust Vib [Internet]. 2016;21(1). Available from: http://dx.doi.org/10.20855/ijav.2016.21.1394
20. Kim H, Lee S, Lee J, Park K-H, Nam S. Enhancing tool wear prediction accuracy by integrating multi-task learning with cutting force estimation. Int J Precis Eng Manuf-Green Technol [Internet]. 2025;12(3):969–89. Available from: http://dx.doi.org/10.1007/s40684-025-00719-y
21. Susac F, Stan F, Fetecau C, Besliu I. Prediction and optimization of surface roughness and cutting force in turning of UHMWPE by using Taguchi method, Response Surface Methodology and neural networks. In: Volume 2: Manufacturing Processes; Manufacturing Systems; Nano/Micro/Meso Manufacturing; Quality and Reliability. American Society of Mechanical Engineers; 2020.
22. Majumder H, Saha A. Application of MCDM based hybrid optimization tool during turning of ASTM A588. Decis Sci Lett [Internet]. 2018;143–56. Available from: http://dx.doi.org/10.5267/j.dsl.2017.6.003
23. Das PP, Chakraborty S. A comparative analysis on optimization of end milling processes using multi-criteria decision making methods. Int J Interact Des Manuf (IJIDeM) [Internet]. 2023;17(4):1611–32. Available from: http://dx.doi.org/10.1007/s12008-023-01209-8
24. Zhang P, Chen Z, Guo L, Li C, Lu S, Sun J. Machining of Invar 36 alloy: Chip-flow behaviors and formation mechanisms. J Manuf Process [Internet]. 2024;132:477–93. Available from: http://dx.doi.org/10.1016/j.jmapro.2024.10.070
25. Khanna N, Gandhi A, Nakum B, Srivastava A. Optimization and analysis of surface roughness for INVAR-36 in end milling operations. Mater Today [Internet]. 2018;5(2):5281–8. Jovicic G, Milosevic A, Kanovic Z, Sokac M, Simunovic G, Savkovic B, et al. Optimization of dry turning of Inconel 601 alloy based on surface roughness, tool wear, and material removal rate. Metals (Basel) [Internet]. 2023;13(6):1068. Available from: http://dx.doi.org/10.3390/met13061068
26. Mahir A. A comparative study on the cutting performance of uncoated, AlTiN and TiCN-Al2 O3 coated carbide inserts in turning of Invar 36 alloy. Journal of Engineering Research and Applied Science. 2022;11(1):2045–61.

27. Jovicic G, Milosevic A, Kanovic Z, Sokac M, Simunovic G, Savkovic B, et al. Optimization of dry turning of Inconel 601 alloy based on surface roughness, tool wear, and material removal rate. Metals (Basel) [Internet]. 2023;13(6):1068.
Available from: http://dx.doi.org/10.3390/met13061068
28. Grynal, Mello NA, Pai PS, Puneet NP, Fang N. Surface roughness evaluation using cutting vibrations in high speed turning of Ti-6Al-4V - an experimental approach. Int J Mach Mach Mater [Internet]. 2016;18(3):288.
Available from: http://dx.doi.org/10.1504/ijmmm.2016.076281
29. Mastan Rao P, Deva Raj C, Dhoria SH, Vijaya M, Chowdary JRR. Multi-objective optimization of turning for nickel-based alloys using Taguchi-GRA and TOPSIS approaches. J Inst Eng (India) Ser D [Internet]. 2024;105(3):1473–84.
Available from: http://dx.doi.org/10.1007/s40033-023-00554-y
30. Eskandari B, Davoodi B, Ghorbani H. Multi-objective optimization of parameters in turning of N-155 iron-nickel-base superalloy using gray relational analysis. J Braz Soc Mech Sci Eng [Internet]. 2018;40(4). Available from: http://dx.doi.org/10.1007/s40430-018-1156-y
31. Abbed K, Kribes N, Yallese MA, Chihaoui S, Boutabba S. Effects of tool materials and cutting conditions in turning of Ti-6Al-4V alloy: statistical analysis, modeling and optimization using CoCoSo, MABAC, ARAS and CODAS methods. Int J Adv Manuf Technol [Internet]. 2023;128(3–4):1535–57.
Available from: http://dx.doi.org/10.1007/s00170-023-11775-6
32. Sivalingam V, Poogavanam G, Natarajan Y, Sun J. Optimization of atomized spray cutting fluid eco-friendly turning of Inconel 718 alloy using ARAS and CODAS methods. Int J Adv Manuf Technol [Internet]. 2022;120(7–8):4551–64.
Available from: http://dx.doi.org/10.1007/s00170-022-09047-w
33. Tan H, Wang Y, Wang G, Zhang F, Fan W, Feng Z, et al. Investigation on microstructure and properties of laser solid formed low expansion Invar 36 alloy. J Mater Res Technol [Internet]. 2020;9(3):5827–39. Available from: http://dx.doi.org/10.1016/j.jmrt.2020.03.108
34. Pan L, Wu ZR, Fang L, Song YD. Investigation of surface damage and roughness for nickel-based superalloy GH4169 under hard turning processing. Proc Inst Mech Eng B J Eng Manuf [Internet]. 2020;234(4):679–91.
Available from: http://dx.doi.org/10.1177/0954405419885789
35. Veerappan G, Pritima D, Parthsarathy NR, Ramesh B, Jayasathyakawin S. Experimental investigation on machining behavior in dry turning of nickel based super alloy-Inconel 600 and analysis of surface integrity and tool wear in dry machining. Mater Today [Internet]. 2022;59:1566–70.
Available from: http://dx.doi.org/10.1016/j.matpr.2022.04.151
36. Lakshmikanthan P, Prabu B. Optimization of CNC turning operations with multiple performance characteristics using Taguchi based grey relational analysis. Int J Veh Struct Syst [Internet]. 2017;9(4). Available from: http://dx.doi.org/10.4273/ijvss.9.4.06
37. Gökkaya H. The effects of machining parameters on cutting forces, surface roughness, Built-Up Edge (BUE) and Built-Up Layer (BUL) during machining AA2014 (T4) alloy. Strojniski Vestnik-journal of Mechanical Engineering. 2010;56(9):584–93.
38. Tan L, Yao C, Li X, Fan Y, Cui M. Effects of machining parameters on surface integrity when turning inconel 718. J Mater Eng Perform [Internet]. 2022;31(5):4176–86.
Available from: http://dx.doi.org/10.1007/s11665-021-06523-4
39. Marakini V, Pai SP, Bhat UK, Thakur D, Achar B. Surface integrity investigation and VIKOR optimisation during the milling of aluminium–lithium alloy using uncoated and PVD-coated carbide tools. Can Metall Q [Internet]. 2024;63(3):767–78.
Available from: http://dx.doi.org/10.1080/00084433.2023.2234137
40. Zhou X, Liu H, Yu T, Guo R, Wang G, Sun Y, et al. Experimental and modeling study of surface topography generation considering tool-workpiece vibration in high-precision turning. Chin J Aeronaut [Internet]. 2023;36(7):194–212.
Available from: http://dx.doi.org/10.1016/j.cja.2022.12.018
41. Samin R, Nuawi MZ, Haris SM, Ghani JA. Stability analysis of regenerative vibration in turning operation using I-kaz3DTM signal processing approach. J Phys Conf Ser [Internet]. 2019;1262(1):012029.
Available from: http://dx.doi.org/10.1088/1742-6596/1262/1/012029
42. Vijayendra S, Marakini V, Pai K. R, Pai P. S, Bolar G. Cryogenic and conventional machining using CVD-coated inserts to improve the surface characteristics of low-carbon steel alloy E350. Cogent Eng [Internet]. 2025;12(1).
Available from: http://dx.doi.org/10.1080/23311916.2025.2525442
43. Pedroso AFV, Sousa VFC, Sebbe NPV, Silva FJG, Campilho RDSG, Sales-Contini RCM, et al. A comprehensive review on the conventional and non-conventional machining and tool-wear mechanisms of INCONEL®. Metals (Basel) [Internet]. 2023;13(3):585. Available from: http://dx.doi.org/10.3390/met13030585
44. Tu L, Ming W, Xu X, Cai C, Chen J, An Q, et al. Wear and failure mechanisms of SiAlON ceramic tools during high-speed turning of nickel-based superalloys. Wear [Internet]. 2022;488–489(204171):204171.
Available from: http://dx.doi.org/10.1016/j.wear.2021.204171
45. Silva F, Martinho R, Martins C, Lopes H, Gouveia R. Machining GX2CrNiMoN26-7-4 DSS alloy: Wear analysis of TiAlN and TiCN/Al2O3/TiN coated carbide tools behavior in rough end milling operations. Coatings [Internet]. 2019;9(6):392. Available from: http://dx.doi.org/10.3390/coatings9060392
46. Hao Z, Cheng G, Fan Y, Li L, Kong L. Research on tool stick-slip erosion wear mechanism in cutting nickel-based alloy GH4169. Tribol Int [Internet]. 2023;188(108803):108803.
Available from: http://dx.doi.org/10.1016/j.triboint.2023.108803
47. Prasad BS, Babu MP. Correlation between vibration amplitude and tool wear in turning: Numerical and experimental analysis. Eng Sci Technol Int J [Internet]. 2017;20(1):197–211. Available from: http://dx.doi.org/10.1016/j.jestch.2016.06.011
48. Tobias SA. Machine-tool vibration. London: Blackie & Son Ltd.; 1965.
49. Quintana G, Ciurana J. Chatter in machining processes: A review. Int J Mach Tools Manuf [Internet]. 2011;51(5):363–76. Available from: http://dx.doi.org/10.1016/j.ijmachtools.2011.01.001
50. Siddhpura M, Paurobally R. A review of chatter vibration research in turning. Int J Mach Tools Manuf [Internet]. 2012;61:27–47. Available from: http://dx.doi.org/10.1016/j.ijmachtools.2012.05.007
51. Dimla DE Snr. Sensor signals for tool-wear monitoring in metal cutting operations—a review of methods. Int J Mach Tools Manuf [Internet]. 2000;40(8):1073–98. Available from: http://dx.doi.org/10.1016/s0890-6955(99)00122-4
52. Xia C, Wu Y, Lu Q. Transversal vibration analysis of an axially moving string with unilateral constraints using the HHT method. Mech Syst Signal Process [Internet]. 2013;39(1–2):471–88. Available from: http://dx.doi.org/10.1016/j.ymssp.2013.01.018

The authors would like to thank NITTE (Deemed to be University) for sponsoring this research project Ref. No.: N(DU)/RD/NUFR2 grant/NMAMIT/2023-24/02.

Sushmith Shetty: https://orcid.org/0009-0002-7981-8333

Vikas Marakini: https://orcid.org/0000-0003-4001-6464

Grynal D'Mello: https://orcid.org/0000-0002-3010-325X

Gururaj Bolar: https://orcid.org/0000-0002-7942-8207